



Lawrence Berkeley Laboratory

UNIVERSITY OF CALIFORNIA

CHEMICAL BIODYNAMICS DIVISION

Submitted to the Journal of Chemical Physics

CIRCULAR INTENSITY DIFFERENTIAL SCATTERING OF LIGHT
BY HELICAL STRUCTURES. III. A GENERAL POLARIZABILITY
TENSOR AND ANOMALOUS SCATTERING.

Carlos Bustamante, Marcos F. Maestre, and
Ignacio Tinoco, Jr.

November 1980

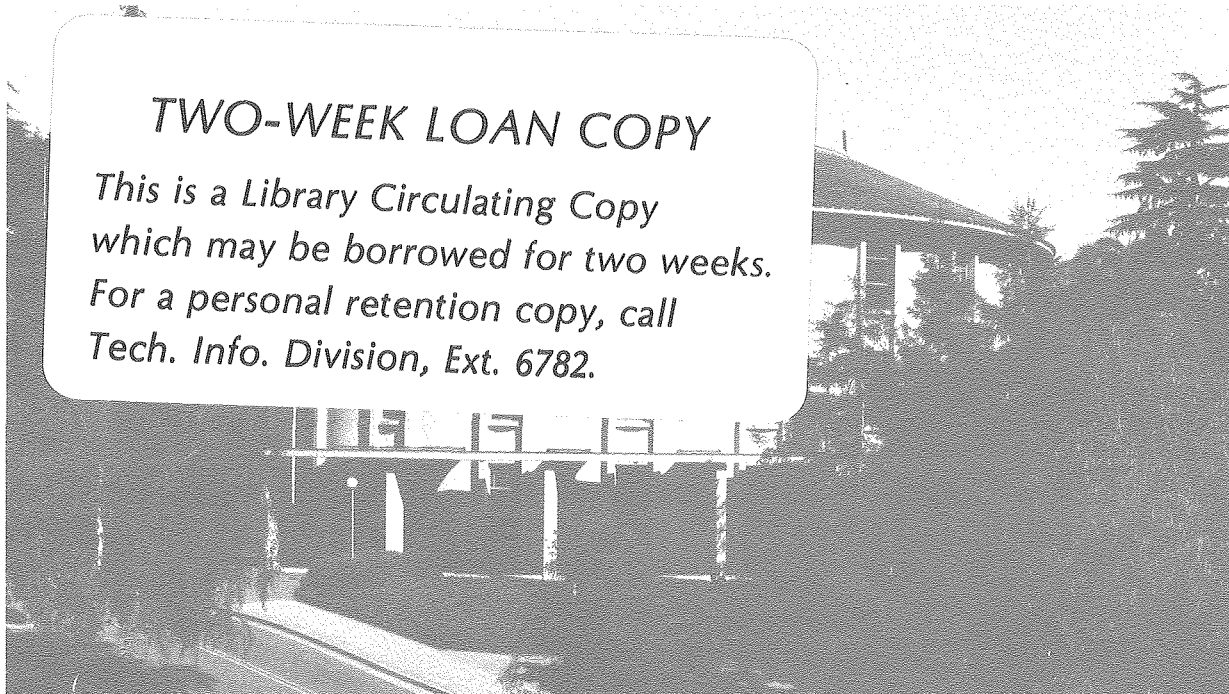
RECEIVED
LAWRENCE
BERKELEY LABORATORY

JAN 8 1981

LIBRARY AND
DOCUMENTS SECTION

TWO-WEEK LOAN COPY

*This is a Library Circulating Copy
which may be borrowed for two weeks.
For a personal retention copy, call
Tech. Info. Division, Ext. 6782.*



LBL-11911 c.2

DISCLAIMER

This document was prepared as an account of work sponsored by the United States Government. While this document is believed to contain correct information, neither the United States Government nor any agency thereof, nor the Regents of the University of California, nor any of their employees, makes any warranty, express or implied, or assumes any legal responsibility for the accuracy, completeness, or usefulness of any information, apparatus, product, or process disclosed, or represents that its use would not infringe privately owned rights. Reference herein to any specific commercial product, process, or service by its trade name, trademark, manufacturer, or otherwise, does not necessarily constitute or imply its endorsement, recommendation, or favoring by the United States Government or any agency thereof, or the Regents of the University of California. The views and opinions of authors expressed herein do not necessarily state or reflect those of the United States Government or any agency thereof or the Regents of the University of California.

Circular Intensity Differential Scattering of Light by Helical Structures.
III. A General Polarizability Tensor and Anomalous Scattering.

Carlos Bustamante,^a Marcos F. Maestre^b and Ignacio Tinoco, Jr.^a

^aDepartment of Chemistry and Laboratory of Chemical Biodynamics

^bDonner Laboratory, Division of Medical Physics

University of California, Lawrence Berkeley Laboratory,

Berkeley, California 94720

Abstract

Numerical calculations of the circular intensity differential scattering of light by oriented helical structures made of units with general polarizability tensors are presented. The effects on the scattering patterns of both absorptive and dispersive properties of the units are illustrated. The differential scattering and the total scattering both show anomalous scattering phenomena; the differential scattering pattern is asymmetric when the wavelength of incident light is within an absorption band. Equations for bi-axial polarizabilities are used to derive the symmetry properties of the differential scattering pattern and to show how this symmetry can be used to determine the right- or left-handed sense of the helical structure. The wavelength dependence of the scattering pattern is obtained for a Lorentzian polarizability.

Introduction

The first two papers in this series^{1,2} dealt with theoretical and computational studies of the differential scattering of right and left circularly polarized light by helices. The helices were assumed to have a uniaxial polarizability tangent to the helix; as a result, the model presented two main features: (1) the values of circular intensity differential scattering (CIDS) were independent of the magnitude of the polarizability, in particular of its wavelength dependence. The model, therefore, did not include any absorptive phenomena. (2) All differential scattering patterns were symmetric around the direction of incidence of the light.²

In this paper we will explicitly analyze the case of a biaxial polarizability and we will also show numerical computations for a general polarizability tensor containing three principal components. Since the model now will give results dependent on the actual form and dispersion properties of the polarizability, we must explicitly consider the wavelength dependence of the polarizability.

Numerical Calculations

Circular intensity differential scattering (CIDS) is the preferential scattering of light of circular polarization by chiral structures. CIDS is defined as the ratio of the difference of scattered intensities for incident left and right circularly polarized light to its sum. $CIDS = (I_L - I_R)/(I_L + I_R)$, where I_L and I_R are the scattered intensities for the two circular polarizations of the incident radiation.

In paper I of this series, the equations for CIDS of helical structure were derived; we use equations 19, 20, A3 and A4 of that paper in the calculations reported here.

We assume that the polarizable electrons in the scatterer are harmonically bound, so that their response to an external field is expressed simply as:³

$$\alpha = \frac{f}{\left(\frac{1}{\lambda_0^2} - \frac{1}{\lambda^2}\right) + \frac{i\Delta\lambda}{\lambda(\lambda_0^2 - \frac{(\Delta\lambda)^2}{4})}} \quad (1)$$

where f is the strength of the absorption band centered at wavelength λ_0 and $\Delta\lambda$ is equal to its width at half height. In the numerical computations we have used polarizability tensors with two or three principal values along principal axes oriented tangent to the helix, t , normal to the helix, n , and perpendicular to these axes, p .¹ Total and differential scattering patterns were calculated as a function of the pitch and radius of the helix, the wavelength of incident light, and for various strengths (f), widths ($\Delta\lambda$), and positions (λ_0) of the absorption bands along the axes defined. Figure 1 shows the results of the total and differential scattering for the case of a triaxial polarizable helix of pitch = 3.6 and radius = 1.1; the wavelength $\lambda = 1.0$, and centers of bands are $\lambda_{0t} = 1.0$, $\lambda_{0n} = 2.0$, $\lambda_{0p} = 1.5$, with strengths, f , all = 1 and widths, $\Delta\lambda = 0.15$. Figure 1b shows the total scattering and the CIDS for a helix of the same dimensions, but with uniaxial (tangential) polarizability. In both cases, +1, 0 and -1 layer lines are shown. The main feature of the general polarizability results is that the differential scattering patterns are now asymmetric when the wavelength of the

incident radiation is within an absorption band of the polarizability. This contrasts with the uniaxial model where the 270° - 90° -axis (see Fig. 1) is a C_2 -axis for each of the layer lines.² For a general polarizability, only the zero layer line has this property. The asymmetry is seen both in the CIDS and in the total scattering; it is called anomalous scattering in X-ray diffraction. One sees in Figure 1a that the +1 and -1 layer lines are the mirror images of each other. A second feature of these general polarizability calculations is that the lobes of differential scattering have decreased in number (compared to the ones appearing in the uniaxial patterns) as well as having become sharper and restricted to smaller domains of the scattering angle ψ . Apparently, each polarizability produces its independent pattern; the superposition of these patterns produces sharper and more localized lobes.

We found that the use of purely real or purely imaginary polarizabilities had the effect of producing total and differential scattering patterns symmetric about the 270° - 90° axis. This is shown in Figure 2 for a helix of the same dimensions as those used in Figure 1 and with the polarizabilities $\alpha_t = \text{Re } \alpha_t$, $\alpha_p = \text{Re } \alpha_p$ and $\alpha_n = \text{Re } \alpha_n$. It should be pointed out that the number of lobes for the zeroth-layer line in Fig. 2 is the same as in the corresponding layer line in Fig. 1a, but here, three negative lobes are too small to be seen in the figure. As discussed in paper II of this series, the number of lobes of the CIDS pattern is determined by the geometry of the scatterer and not by the values and directions of the transitions in the scatterer. In order to gain a better understanding of the symmetry laws involved in the patterns of total and differential scattering, the theory of CIDS for helical molecules is explicitly applied to the case of a biaxial polarizability.

It will be shown that by writing the polarizabilities in the form $\alpha = R \exp(i\gamma)$, a phase change is introduced in the angular dependence of the scattering intensity, which is equal to the difference in the complex phases between the polarizabilities involved; this phase change is responsible for the antisymmetric properties observed. A detailed analysis of the symmetry of the scattering patterns will show their relations to the dispersive and absorptive properties of the polarizabilities.

A Biaxial Polarizability

We choose a biaxial polarizability with principal axes along \underline{n} and \underline{t} . We can define the scattering matrix for the helix as:

$$S = F(1 - \hat{k}\hat{k}) \int_{-\lambda\pi}^{\lambda\pi} e^{i\mathbf{k}\cdot\mathbf{r}} (\alpha_{\underline{t}\underline{t}} + \alpha_{\underline{n}\underline{n}}) d\theta \quad (2)$$

where $\hat{k} = \underline{k}/|\underline{k}|$ is a unit vector along the direction of scattering, F includes constants and distance dependent factors, λ is the number of turns of the helix, $\alpha_{\underline{t}}$ and $\alpha_{\underline{n}}$ are the magnitudes of the principal polarizabilities, and \underline{r} is the vector position of the segments in the scatterer.

The electric field of the scattered light for right circularly polarized light and left circularly polarized incident light with polarization vector defined by $(\underline{e}_3 + i\underline{e}_1)$ and $(\underline{e}_3 - i\underline{e}_1)$, respectively, and incident wave-vector \underline{k}_0 along \underline{e}_2 (y-axis) is:

$$\underline{E} = F(1 - \hat{k}\hat{k}) \cdot \int_{-\lambda\pi}^{\lambda\pi} e^{i\Delta\mathbf{k}\cdot\mathbf{r}} [\alpha_{\underline{t}\underline{t}}(\underline{t}\cdot\underline{e}_3) + \alpha_{\underline{n}\underline{n}}(\underline{n}\cdot\underline{e}_3) \pm i(\alpha_{\underline{t}\underline{t}}(\underline{t}\cdot\underline{e}_1) + \alpha_{\underline{n}\underline{n}}(\underline{n}\cdot\underline{e}_1))] d\theta \quad (3)$$

The plus sign gives the scattered field for right circularly polarized light and the minus sign for left circularly polarized light, with $\Delta \underline{k} = \underline{k} - \underline{k}_0$. For a helix oriented along \underline{e}_3 ($\underline{n} \cdot \underline{e}_3 = 0$), we can write the terms that must be added to the ones calculated with the purely tangential polarizability¹ to obtain $I_L - I_R$. These additional terms are:

$$E_L E_L^* - E_R E_R^* = 4F^2 \{ \iint \text{Im}(\alpha_t^* \alpha_n e^{i\Delta \underline{k} \cdot (\underline{r} - \underline{r}')}) (\underline{n} \cdot \underline{t}') (\underline{t}' \cdot \underline{e}_3) (\underline{n} \cdot \underline{e}_1) d\theta d\theta' + \iint \text{Im}(\alpha_t^* \alpha_n e^{i\Delta \underline{k} \cdot (\underline{r} - \underline{r}')}) (\underline{t} \cdot \hat{\underline{k}}) (\underline{t} \cdot \underline{e}_3) (\underline{n}' \cdot \hat{\underline{k}}) (\underline{n}' \cdot \underline{e}_1) d\theta d\theta' \} \quad (4)$$

where Im means the imaginary part of the expression should be used, and where the limits of integration have been omitted for simplicity. To perform the integrations indicated in (4), we rewrite the polarizabilities α_t and α_n as $\alpha_t = R_t e^{i\gamma_t}$ and $\alpha_n = R_n e^{i\gamma_n}$ where R_t , R_n , γ_t and γ_n are real numbers. In this way, after integration, we obtain the correction terms for $I_L - I_R$ that can be found in the appendix at the end of the paper. Here we will only show one of the terms obtained, to allow the analysis of the symmetries involved:

$$\frac{k_x k_z p^2}{4\pi^2 M^2} [J_n J_{n-2} \sin(2\psi' + (\gamma_t - \gamma_n)) - J_n J_{n+2} \sin(2\psi' - (\gamma_t - \gamma_n))] \quad (5)$$

(5-1)

(5-2)

where the arguments of the Bessel functions, which are (Qa) , the angle ψ' and constant M have the same definition as in paper I, and k_z and k_x are the e_3 and e_1 components of the scattered wave-vector, respectively.

Symmetry Analysis

In all the correction terms, the use of a multiaxial polarizability has the effect of introducing phase changes $(\gamma_t - \gamma_n)$ in the trigonometric functions of the scattering angle ψ and related angles ψ' . These phase shifts are related to the scattering patterns which show differential and total scattering intensities in more restricted and smaller domains of the scattering angle ψ as discussed above. It is therefore clear that the new symmetry properties must be contained in the cross terms of \underline{t} and \underline{n} (equations in Appendix), and consequently, our analysis does not have to consider the contribution to the scattering intensities of the purely tangential solution given in paper I. Figure 3 shows a diagrammatic description of the symmetries involved in the differential and total anomalous scattering. The lines drawn from the scatterer to the plane A represent actual directions of the wave vector of the scattered light. Any point in the plane, therefore, where nonvanishing differential or total scattering is observed, can be described completely by the coordinates (k_x, k_z) , its sign of polarization (in the case of the differential scattering), and the observed intensity at that point. One sees that the point 0 represents an inversion point for the pattern in plane A, the differential or total scattered intensities of the point (k_x, k_z) being the same as that of $(-k_x, -k_z)$, and that of $(-k_x, k_z)$ being the same as that of $(k_x, -k_z)$. Through our symmetry analysis of the differential scattering, we should be able to show the exis-

tence of the following properties: (a) when the polarizabilities are purely real or imaginary, the patterns must be invariant for a change of $k_x \rightarrow -k_x$ and will also be invariant for a change $k_z \rightarrow -k_z$. (b) When the polarizabilities are complex, the equations should be invariant only for a simultaneous transformation of $k_x \rightarrow -k_x$ and $k_z \rightarrow -k_z$. (c) The zeroth-layer line is completely symmetric to independent changes of $k_x \rightarrow -k_x$ and to changes of $k_z \rightarrow -k_z$ regardless of the use of complex polarizabilities. (d) The total scattering shows the same asymmetric behavior as the differential scattering.

Equation (5) can be rewritten as:

(6)

$$\frac{k_x k_z}{4\pi^2 M^2} P^2 \{ (J_{n-2} J_n - J_n J_{n+2}) \sin 2\psi' \cos \delta + (J_{n-2} J_n + J_n J_{n+2}) \cos 2\psi' \sin \delta \}$$

(6-1)

(6-2)

with $\delta = \gamma_t - \gamma_n$.

Equation (6) has the general form:

$$C_{1x} C_{1z} P_1 B_1 \cos \delta + C_{2x} C_{2z} P_2 B_2 \sin \delta$$

where C stands for coefficient, P for phase ($\sin 2\psi'$ or $\cos 2\psi'$ in this case) and B for the combination of Bessel functions. Some of the terms are affected by changes of the x-coordinate and some by changes in the z-coordinate. It can be shown that the above term, under the double reflection ($x \rightarrow -x$; $z \rightarrow -z$) transforms as:

$$C_{1x}C_{1z}P_1B_1\cos\delta + C_{2x}C_{2z}P_2B_2\sin\delta$$

$$\begin{pmatrix} + \\ \downarrow \\ - \end{pmatrix} \begin{pmatrix} + \\ \downarrow \\ - \end{pmatrix} \begin{pmatrix} + \\ \downarrow \\ - \end{pmatrix} \begin{pmatrix} + \\ \downarrow \\ - \end{pmatrix} \quad \begin{pmatrix} + \\ \downarrow \\ - \end{pmatrix} \begin{pmatrix} + \\ \downarrow \\ - \end{pmatrix} \begin{pmatrix} + \\ \downarrow \\ + \end{pmatrix} \begin{pmatrix} + \\ \downarrow \\ + \end{pmatrix} \quad (7)$$

where the terms affected by changes of $k_z \rightarrow -k_z$ are shown in square brackets and the ones affected by changes of $k_x \rightarrow -k_x$ are in parenthesis. From expressions (7) and (6) we see that term (6-1) is symmetric with respect to changes of $k_x \rightarrow -k_x$ as well as to changes of $k_z \rightarrow -k_z$, whereas (6-2) is antisymmetric with respect to either two of these transformations. This different behavior of the two terms is responsible for the asymmetry observed in the differential patterns. When the polarizabilities are purely real, then $\delta = 0$, and the asymmetric term vanishes, leaving only the terms 6-1 invariant to changes $k_x \rightarrow -k_x$ as well as to changes in $k_z \rightarrow -k_z$. Similarly, when purely imaginary polarizabilities are used, this means that $\gamma_t = (2n_t + 1)\pi/2$ and $\gamma_n = (2n_n + 1)\pi/2$ for $n_t, n_n = 0, 1, 2, \dots$, therefore the difference $\delta \equiv \gamma_t - \gamma_n = 2(n_t - n_n)\pi/2$ and $\sin\delta \equiv 0$, leaving again in this case only the symmetric terms. When the polarizabilities involved are complex, it is clear from (6) that the term will still be symmetric for the simultaneous transformation ($k_x \rightarrow -k_x; k_z \rightarrow -k_z$). Finally, in the zeroth-layer line, even though the polarizabilities might be complex, this term vanishes, either because $k_z = 0$ in the zeroth layer line, or because the Bessel term B evaluated at $n = 0$ vanishes. Expression (6) contains, therefore (as does each one of the remaining terms of the correction of $I_L - I_R$; see equations in the Appendix), all the antisymmetric properties depicted by the differential scattering pattern. Essentially, the same findings are applicable to the symmetry

properties of the total scattering (see Figure 1). The correction terms for the total ($I_L + I_R$) scattering can be obtained from expression (3). Squaring the amplitudes of opposite circular polarization and adding them, after some algebra, we obtain a formal expression for the correction term as:

$$I_L + I_R = 2F^2 \{ R_n^2 \iint e^{i\Delta k \cdot (r-r')} (\underline{n}' \cdot \underline{e}_1) (\underline{n} \cdot \underline{e}_1) [\underline{n}' \cdot (\underline{1} - \hat{k}\hat{k}) \cdot \underline{n}'] d\theta d\theta' \quad (8)$$

$$+ 2R_t R_n \iint \cos(\Delta k \cdot (r-r') + (\gamma_t - \gamma_n)) (\underline{t} \cdot \underline{e}_1) (\underline{n}' \cdot \underline{e}_1) [\underline{n}' \cdot (\underline{1} - \hat{k}\hat{k}) \cdot \underline{t}] d\theta d\theta' \}$$

where \underline{n}' and \underline{n} indicate the normal axes of the polarizabilities; they are functions of the variables θ' and θ , respectively.

Equation (8) shows that the total scattering involves a cross-term of the values of the polarizability along the two axes \underline{t} and \underline{n} , and includes the phase difference $\delta \equiv (\gamma_t - \gamma_n)$; this accounts for the antisymmetry shown by the total scattering patterns. Clearly, if the polarizability is spherically symmetric, then the phase changes $(\gamma_t - \gamma_n)$, $(\gamma_t - \gamma_p)$, etc., will all vanish and the patterns will regain their symmetry. This behavior is indeed shown in Figure (4), where all three principal values of the polarizability are identical. The total scattering patterns appear symmetric, while the differential scattering patterns vanish as expected.¹ All the results derived so far are completely general and do not depend on the particular form chosen for the polarizability. In the next section, an analysis of the wavelength dependence of the differential scattering intensities will be done for the Lorentzian polarizability of equation (1). Although the details of the expansions are only valid for this par-

ticular case, most of the conclusion will be valid for a Gaussian shaped band as well.

The Dispersion Dependence of the Scattering Intensities

We have shown above that the use of complex polarizabilities, i.e., allowing for the scatterer to possess absorptive as well as refractive properties, has the effect of producing scattering patterns which are quite asymmetric. The axis defined by the direction of incidence of light in the zeroth-layer line is a C_2 -axis for all the layer lines of scattered intensities in space (i.e., for the overall scattering pattern); but aside from the zeroth layer line, the remaining layer lines have lost their biaxial symmetry in the direction 270° - 90° (see figures). In all the computations we have presented, the simple, harmonically bound electron model has been used for the dispersion properties of the polarizability. Here, starting from expression (1), we will derive the wavelength dependence of the scattering intensities for this Lorentzian-shaped polarizability. Expression (1) can be rewritten as:

$$\alpha = f \left(\frac{1}{\lambda_0} - \frac{1}{\lambda} \right) / \left[\left(\frac{1}{\lambda_0} - \frac{1}{\lambda} \right)^2 - \frac{\Delta\lambda^2}{\lambda^2 \left(\lambda_0^2 - \left(\frac{\Delta\lambda}{2} \right)^2 \right)^2} \right] - \frac{if\Delta\lambda}{\lambda \left(\lambda_0^2 - \left(\frac{\Delta\lambda}{2} \right)^2 \right)} /$$

$$\left[\left(\frac{1}{\lambda_0} - \frac{1}{\lambda} \right)^2 - \frac{\Delta\lambda^2}{\lambda^2 \left(\lambda_0^2 - \left(\frac{\Delta\lambda}{2} \right)^2 \right)^2} \right] \quad (9)$$

From this expression we see that in resonance, $\lambda_0 = \lambda$, and the polarizability becomes purely imaginary. In view of the results presented above, for wavelengths of light corresponding to the center

of the absorption band, completely symmetric scattering patterns must be observed for $I_L - I_R$ as well as for $I_L + I_R$, if the polarizability has a single absorption band common to all axes. Away from the absorption band the anomalous behavior of the scattering disappears. We must show, therefore, that the phase difference $\delta = \gamma_t - \gamma_n$, responsible for the antisymmetry of the patterns, vanishes at wavelengths far outside the absorption bands. To demonstrate this we compare the polarizability $\alpha = R(\cos\gamma + i \sin\gamma)$ with Eq. (9) to obtain an expression for the phase angle γ .

$$\tan \gamma = \frac{\frac{-\Delta\lambda}{\lambda(\lambda_0^2 - [\Delta\lambda/2]^2)}}{\left(\frac{1}{\lambda_0^2} - \frac{1}{\lambda^2}\right)} \approx \frac{-\Delta\lambda}{\lambda} \ll 1 \text{ (away from absorption band)}$$

$$\text{and } \delta \equiv (\gamma_t - \gamma_n) \cong (\Delta\lambda_n - \Delta\lambda_t)/\lambda \approx 0 \text{ (away from the absorption band)} \quad (10)$$

This is the result we were seeking and it shows indeed that far away from the absorption band the antisymmetric terms (proportional to $\sin \delta$) vanish, and symmetric patterns of scattering result. Figures (5a) and (5b) show in fact that this is the case (see details in Figure Caption). By using essentially the same approximations, from Eq. (9) it can be shown that away from resonance:

$$\begin{aligned} \text{Re } \alpha &= f[1 + C_{\lambda_0}^2/(\lambda^2 - \lambda_0^2)] & \text{and} \\ \text{Im } \alpha &= \frac{C_{\lambda_0}}{\lambda\lambda_0(\lambda^2 - \lambda_0^2)} (\text{Re } \alpha) & \text{with } C_{\lambda_0} = \frac{\Delta\lambda}{\lambda_0} \end{aligned} \quad (11)$$

From this last expression we see that in a first approximation, away from resonance, the contribution of the imaginary part of the polarizability to the scattered fields is λ^{-4} times smaller than that of the real part and therefore the imaginary part will not contribute significantly to the scattering intensities, for regions of the spectrum outside of the absorption band.

Discussion

The asymmetry observed in the scattering patterns is the result of having chosen for the scatterer a general polarizability. As discussed in paper I of this series, this choice implies that in calculating the CIDS, the dispersion dependence of the polarizability cannot be cancelled when the ratio of $I_L - I_R$ to $I_L + I_R$ is taken. The effect is to make the calculated differential scattering intensities, as well as the total scattering, dependent on the absorptive properties of the scatterer. This behavior is a manifestation of "anomalous scattering" described in crystallography.⁴ Thus, Friedel's law of symmetry of the scattered intensities above and below the equator of the diffraction pattern is violated when the wavelength of the incident radiation falls inside the absorption band of some of the scattering elements in the lattice. As the wavelength of light moves away from the absorption band, the asymmetry gradually disappears to eventually recover the symmetry of the pattern far away from resonance. However, the antisymmetry shown by the absorptive helix is a property peculiar to the geometry and symmetry of the scatterer studied. In this way, whereas the asymmetry of the scattering patterns is a general manifestation of anomalous scattering, the antisymmetry shown by the patterns is peculiar to the highly symmetric chiral scatterer discussed.

It is well known that the phenomenon of anomalous scattering is used in crystallography as a method to determine the absolute configuration of the scatterers and to recover the phases of the scattered fields.⁵ In Figure 6 the CIDS of a left-handed helix for layer lines +1, 0 and -1 is depicted. It should be compared with the corresponding layer lines in Figure 1. It is seen that the total scattering has a reflection plane defined by the direction of the incident light, and perpendicular to the plane of the figure. The CIDS, on the other hand, gets reflected through this plane as well as changes sign when a transformation from a right to a left-handed helix is done. This effect is important, since it can immediately be used to determine the sense of the helix. Shown in Figure 7 is the effect on the scattering of light incident perpendicular to the helix axis and plane polarized along the axis of the helix (IPOLZ) and perpendicular to it (IPOLX). Again here the scattered intensities are asymmetric and different for the two different polarizations. For a left-handed helix the patterns invert as expected.

Anomalous scattering is a phenomenon known to be independent of the state of polarization of the incident radiation, and therefore independent of the symmetry properties of the polarizability. On the other hand, we have shown that the assumption of spherically symmetric polarizabilities in our case eliminates all the anomalous behavior of the scatterer. The reason for this apparent conflict is that anomalous scattering is independent of the symmetry properties of the polarizability only when some, but not all, of the scattering elements of the unit cell are anomalous scatterers. If all of them are anomalous scatterers, then the violations of Friedel's Law will take place only if the polar-

izability of the scatterers is nonspherically symmetric.⁶ This last case corresponds to our choice for the helix. It must be pointed out that the model of absorptive scattering that has been described above must still be described as FORM-CIDS, since no asymmetrically coupled radiation elements have been included in the model.

Qualitatively, the asymmetry observed in the scattering patterns is the result of a breakdown in the symmetry of the form contribution to the scattering. By allowing absorption bands to be present along the optical axes of the polarizability, the helix scatters with a different efficiency, according to the position of the point in the scatterer excited by the front wave of the incident radiation. The symmetry observed in the nonabsorptive case corresponds to equal scattering efficiency of the points on the scatterer.² The dispersive equations derived for the CIDS in this paper should give information about the handedness of the helical (chiral) structure as well as about the symmetry properties of the polarizability.

Acknowledgments

This work was supported in part by National Institutes of Health Grants GM 10840 (IT) and AI 08247 (MFM) and by the Environmental Research and Development Division of the U.S. Department of Energy under Contract No. W-7405-ENG-48.

Appendix

The integration of equation (4) allows us to calculate the contributions of the cross-terms involving both the tangential and normal axes of the polarizability, to the differential scattering. The terms which only contain \underline{t} have been presented before,¹ whereas in taking the difference the terms in \underline{n} cancel. The correction terms for $I_L - I_R$ for a biaxial polarizability along \underline{t} and \underline{n} axes are therefore

$$\begin{aligned}
 & F_{\underline{t}R}^2 R_n \left\{ \frac{aP}{4\pi M^2} [(2J_{n-1}J_{n-2} - J_n J_{n+1})\cos(\psi'+\delta) - (2J_{n+1}J_{n+2} - J_n J_{n-1})\cos(\psi'-\delta)] \right. \\
 & \frac{k_x^2 aP}{4\pi M^2} [J_{n+1}J_{n-2}\cos(3\psi'+\delta) + (2J_n J_{n+1} - J_{n-1}J_{n-2})\cos(\psi'+\delta) - J_{n+2}J_{n-1}\cos(3\psi'-\delta) \\
 & \left. - (2J_n J_{n-1} - J_{n+2}J_{n+1})\cos(\psi'-\delta) \right] \\
 & \frac{+k_x k_y aP}{2\pi M^2} [J_{n+1}J_{n-2}\sin(3\psi'+\delta) - J_{n+2}J_{n-1}\sin(3\psi'-\delta) + J_{n+1}J_n \sin(\psi'+\delta) \\
 & \left. - J_n J_{n-1}\sin(\psi'-\delta) \right] \\
 & \frac{+k_y^2 aP}{4\pi M^2} [J_{n+2}J_{n-1}\cos(3\psi'-\delta) - J_{n+1}J_{n-2}\cos(3\psi'+\delta) + J_{n+2}J_{n+1}\cos(\psi'-\delta) \\
 & \left. - J_{n-1}J_{n-2}\cos(\psi'+\delta) \right] \\
 & \frac{+k_x k_z P^2}{4\pi^2 M^2} [J_{n-2}J_n \sin(2\psi'+\delta) - J_n J_{n+2}\sin(2\psi'-\delta)] \\
 & \left. \frac{+k_z k_y P^2}{4\pi^2 M^2} [J_n J_{n+2}\cos(2\psi'-\delta) - J_n J_{n-2}\cos(2\psi'+\delta)] \right\}
 \end{aligned}$$

The argument of the Bessel functions is Qa . (See text for the definition of this variable.)

Figure Captions

Figure 1a: Polar plots of intensity vs. scattering angle ψ showing the +1, 0 and -1 layer lines (LYR) of the CIDS and total scattered intensities (SCATT Y) for light incident along the y-axis (from right to left along 270° on the 0 layer line). The parameters are pitch $P = 3.6$, radius $R = 1.1$, wavelength $W = 1.0$, length $L = 20$ turns and a triaxial polarizability band $\lambda_{0p} = 1.5$ and a normal band $\lambda_{0n} = 2.0$. The strengths of the bands are all 1.0 and their half height width chosen equal to 0.15. Heavy and light lines indicate negative and positive values of CIDS, respectively.

Figure 1b: The corresponding polar plots of the same helix as in Figure 1a but having a uniaxial polarizability along the tangential direction with $\lambda_{0t} = 1.0$, band strength = 1.0 and width = 0.15 as before. Notice that both the CIDS and the total scattering away from the zero-layer line have regained their symmetry across the 270° - 90° axis. As in Figure 1a, the negative values are depicted with heavier lines.

Figure 2: Polar plots for the same helix as in Fig. 1a, with a triaxial polarizability, but with $\alpha_t = \text{Re } \alpha_t$, $\alpha_p = \text{Re } \alpha_p$ and $\alpha_n = \text{Re } \alpha_n$. Everything else in the calculation was the same as in Fig. 1a. The CIDS and the total scattering are completely symmetric across the 270° - 90° axis.

Figure 3: Graphic depiction of the anti-symmetry involved in the anomalous scattering of plane or circularly polarized light by a chiral structure. The plane A can be a photographic plate, for example. The point O labels the direction of forward scattering and it represents an inversion point for the intensities recorded at the plate.

Figure 4: Polar plots for the total scattering for a helix with the same structural parameters as those of Fig. 1a, but possessing a spherically symmetric polarizability with $\lambda_{0t} = \lambda_{0p} = \lambda_{0n} = 0.85$, band strengths = 1.0 and band widths = 0.15. The CIDS patterns are all zero. The total scattering appears symmetric as expected (see text).

Figure 5a: Plots of CIDS and total scattering for the +1, 0 and -1 layer lines for a helix of $P = 12$, $R = 0.6$, $L = 20$ turns. The wavelength of light $W = 6.0$ coincides with the center of the tangential band (λ_{0t}) and is close to the perpendicular $\lambda_{0p} = 6.20$ and the normal band $\lambda_{0n} = 5.00$. The band strengths are 1.0 for all three bands and the widths are 0.30. Notice that the +1 and the -1 layer lines are asymmetric for the CIDS as well as the total scattering.

Figure 5b: Equivalent plots to those of Fig. 5a for the same ratios of pitch/wavelength and radius/wavelength and the same band positions. However, the wavelength of light is $W = 10.0$,

i.e., away from any of the absorption bands of the scatterer. The widths and strengths of the bands are the same as in Fig. 5a. CD/MAX indicate that the CIDS intensities have been normalized to 1.0 in this case and therefore cannot be compared to the CIDS values of Fig. 5a, on a quantitative basis. The patterns, as discussed in the text, are all symmetric.

Figure 6: The effect of going from a right- to a left-handed helix can be observed by comparing this figure to Figure 1a. A left-handed helix is obtained by using a negative pitch ($P = -3.6$, in this case). Everything else is the same as in Figure 1a. The total intensities get reflected through a plane containing the 270° - 90° axis and perpendicular to the plane of the figure, whereas the CIDS is reflected and has changed sign. The zero layer line is the same in both the CIDS and the total scattering but the sign of the CIDS is changed.

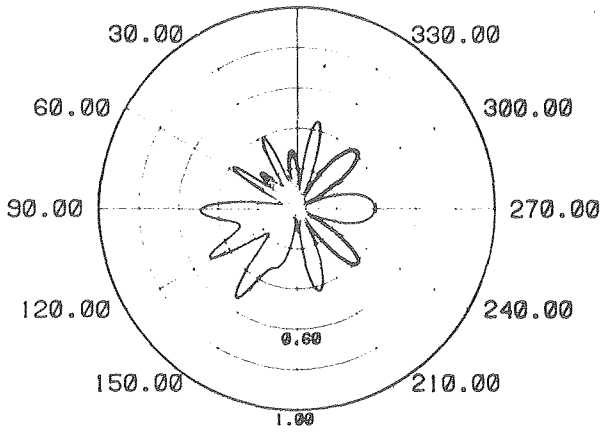
Figure 7: The figure illustrates the fact that plane polarized light can be used to determine the handedness of associated scatterer when the wavelength of light falls within an absorption band. Only the +1 layer line is shown. The zero layer line is symmetric and indistinguishable for the right and left-handed helices.

References

- ¹C. Bustamante, M. F. Maestre, and I. Tinoco, Jr., J. Chem. Phys.,
in press (1980).
- ²C. Bustamante, M. F. Maestre, and I. Tinoco, Jr., J. Chem. Phys.,
in press (1980).
- ³L. Rosenfeld, Theory of Electrons (Dover, New York, 1965).
- ⁴D. Sherwood, Crystals, X-Rays and Proteins (Longman, New York, 1976).
- ⁵E. Lipson and W. Cochran, The Determination of Crystal Structure
(G. Bell & Sons, Ltd., London, 1966).
- ⁶C. Bustamante, Ph.D. Thesis, University of California, Berkeley (1980).

P=3.60 R=1.10
W=1.00 L=20.0

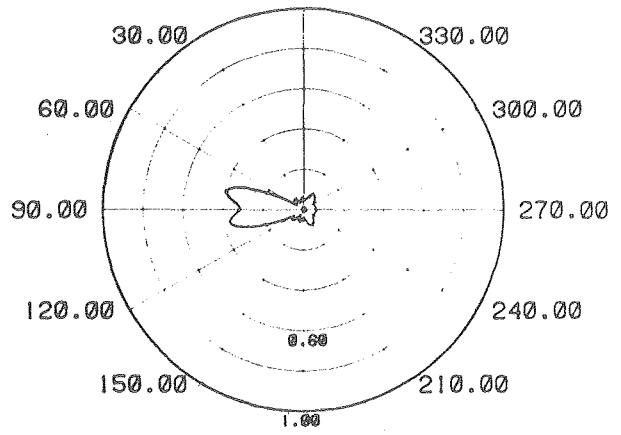
0.00



CIDS Y 180.00 LYR= 1.00

P=3.60 R=1.10
W=1.00 L=20.0

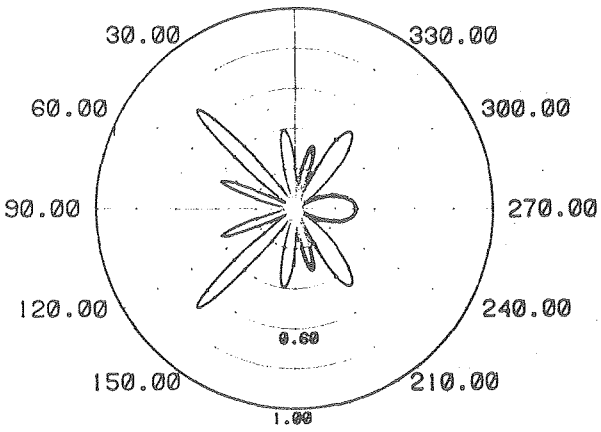
0.00



SCATT Y 180.00 LYR= 1.00

P=3.60 R=1.10
W=1.00 L=20.0

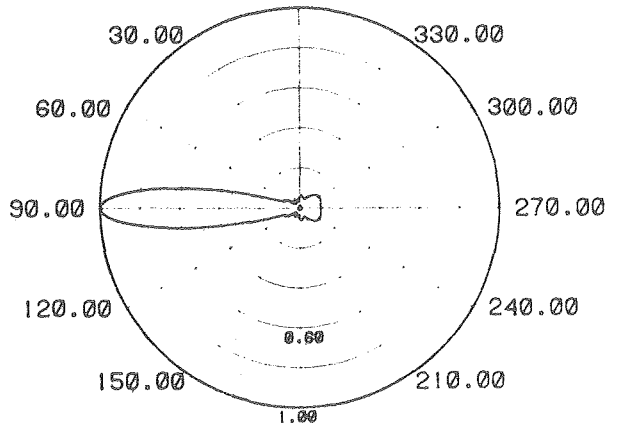
0.00



CIDS Y 180.00 LYR= 0.

P=3.60 R=1.10
W=1.00 L=20.0

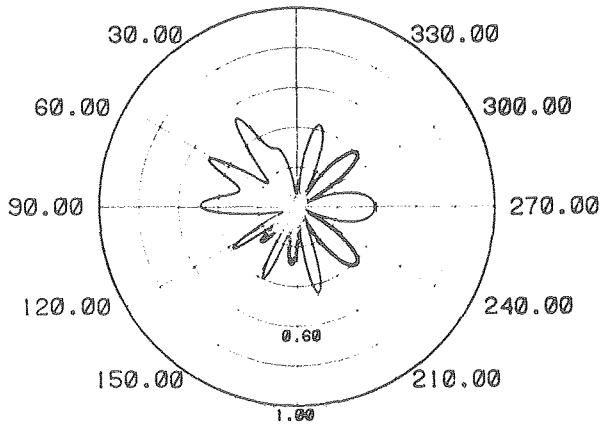
0.00



SCATT Y 180.00 LYR= 0.

P=3.60 R=1.10
W=1.00 L=20.0

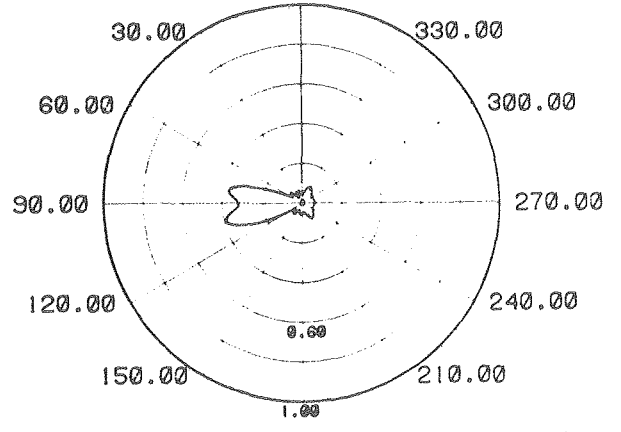
0.00



CIDS Y 180.00 LYR=-1.00

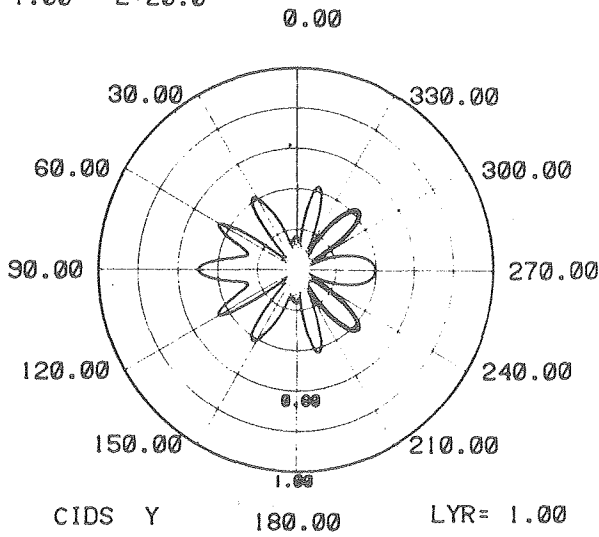
P=3.60 R=1.10
W=1.00 L=20.0

0.00

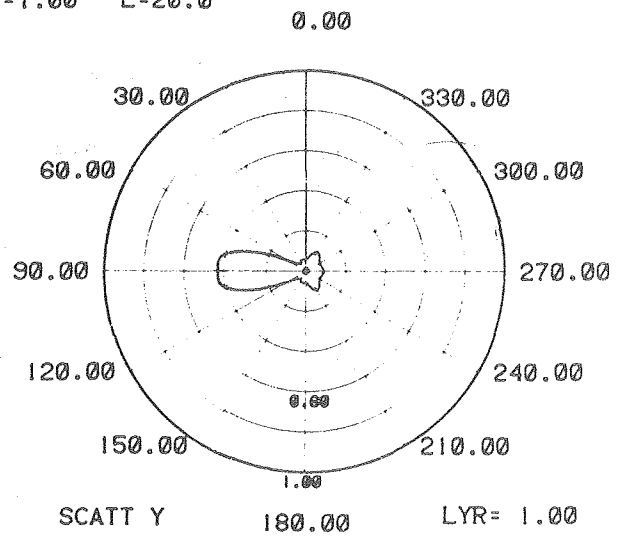


SCATT Y 180.00 LYR=-1.00

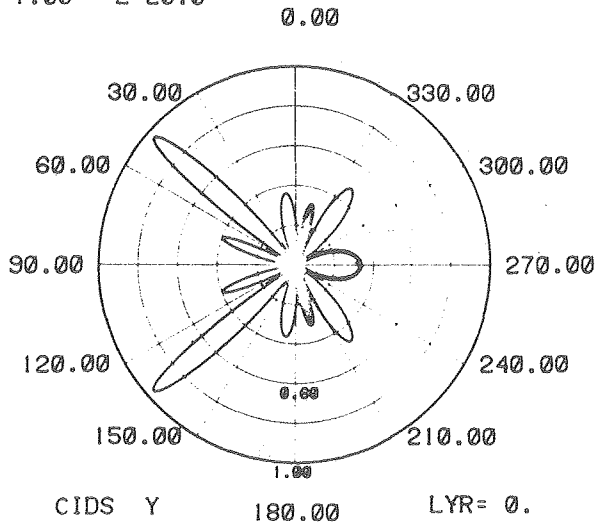
P=3.60 R=1.10
W=1.00 L=20.0



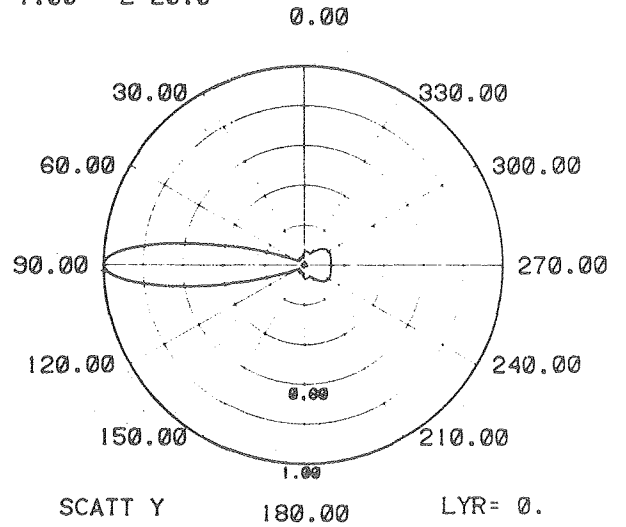
P=3.60 R=1.10
W=1.00 L=20.0



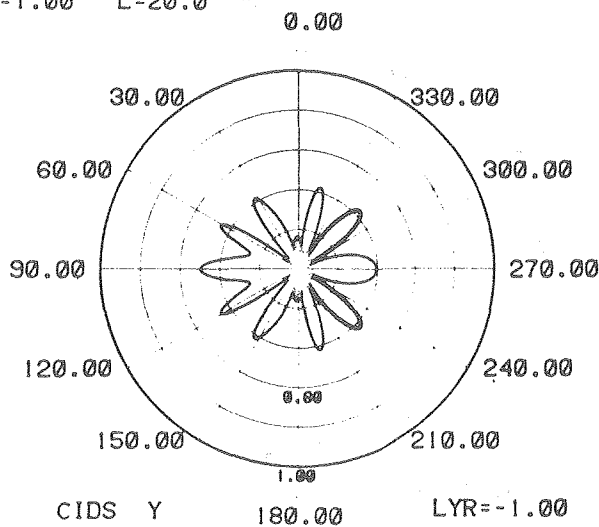
P=3.60 R=1.10
W=1.00 L=20.0



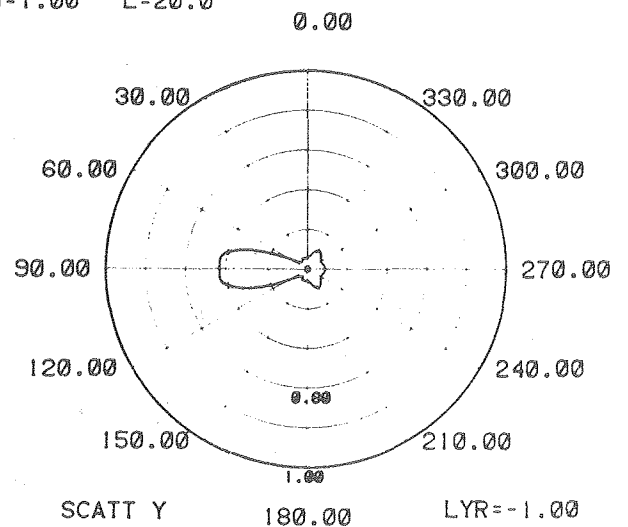
P=3.60 R=1.10
W=1.00 L=20.0



P=3.60 R=1.10
W=1.00 L=20.0

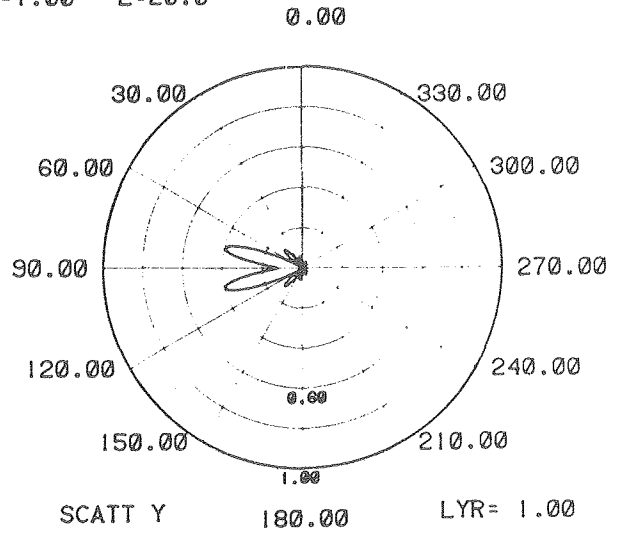
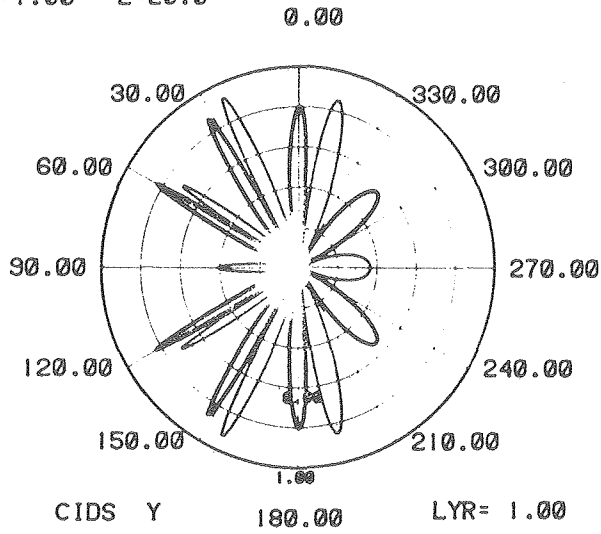


P=3.60 R=1.10
W=1.00 L=20.0



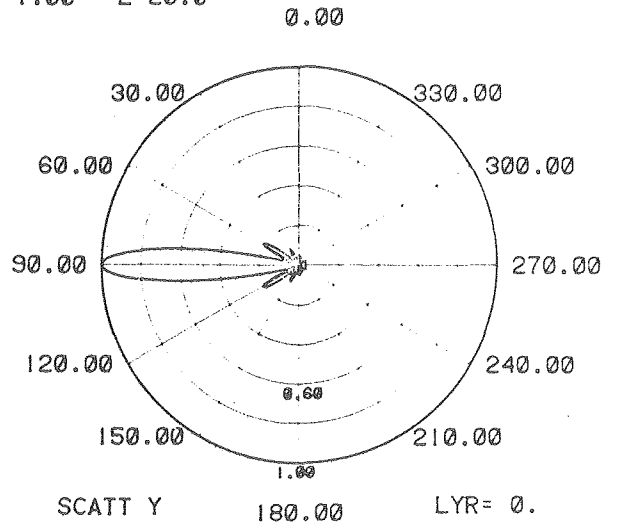
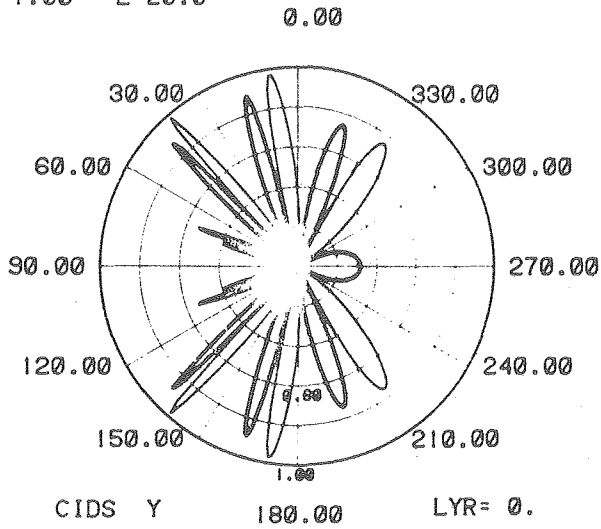
P=3.60 R=1.10
W=1.00 L=20.0

P=3.60 R=1.10
W=1.00 L=20.0



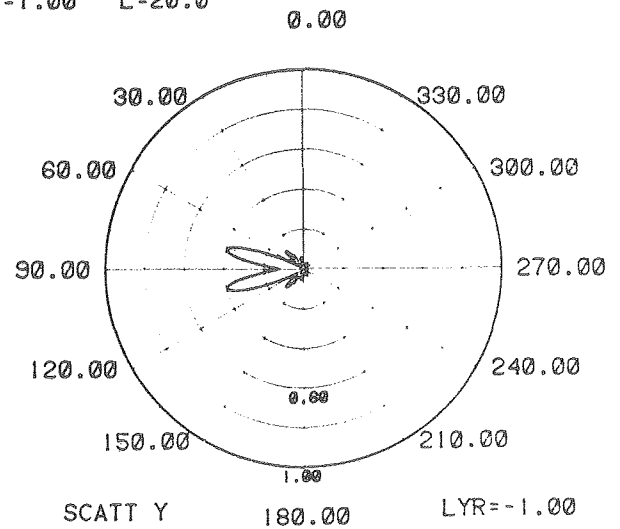
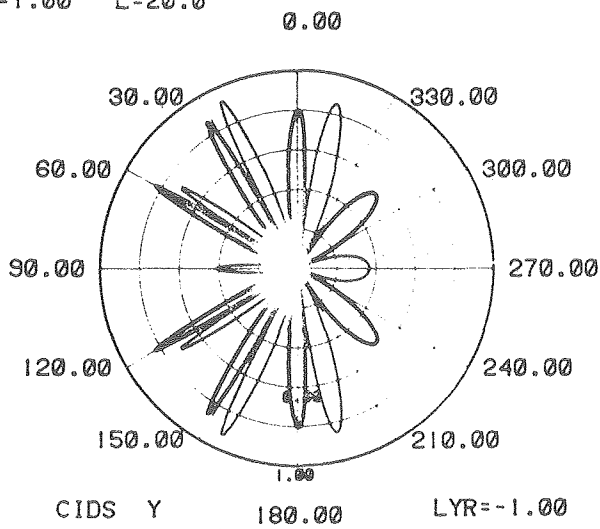
P=3.60 R=1.10
W=1.00 L=20.0

P=3.60 R=1.10
W=1.00 L=20.0



P=3.60 R=1.10
W=1.00 L=20.0

P=3.60 R=1.10
W=1.00 L=20.0



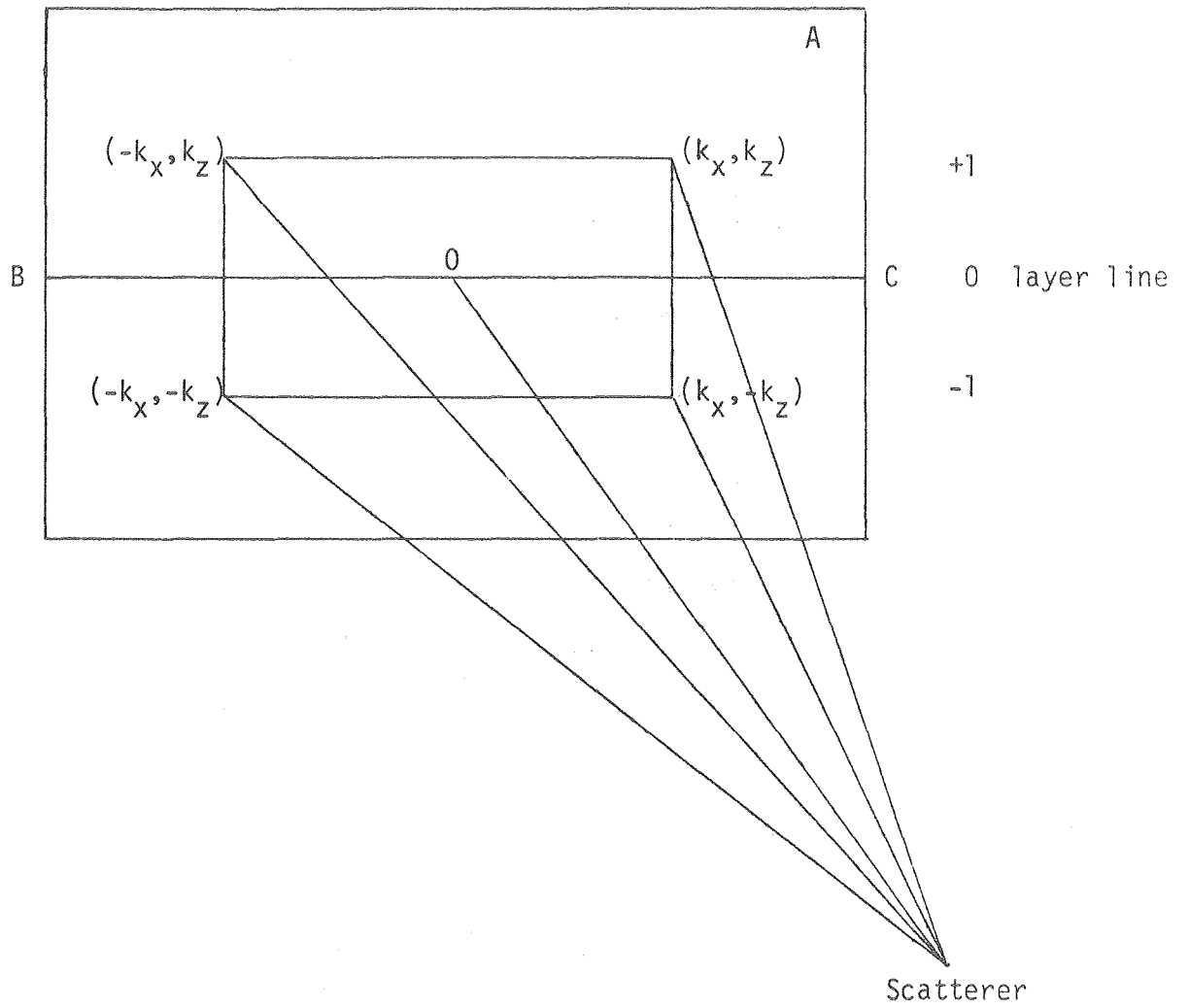
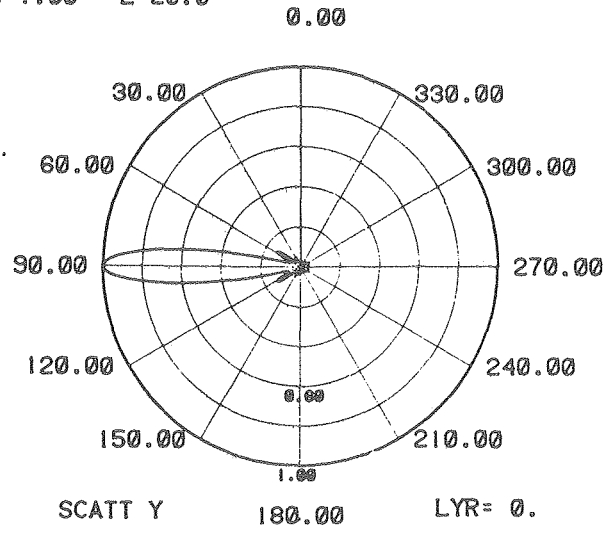
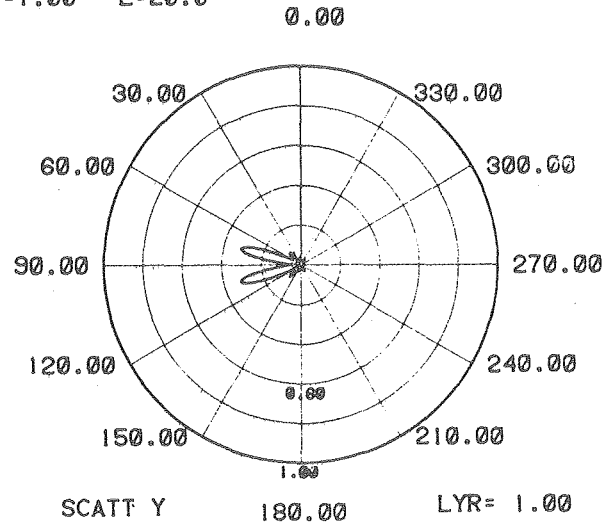


Figure 3

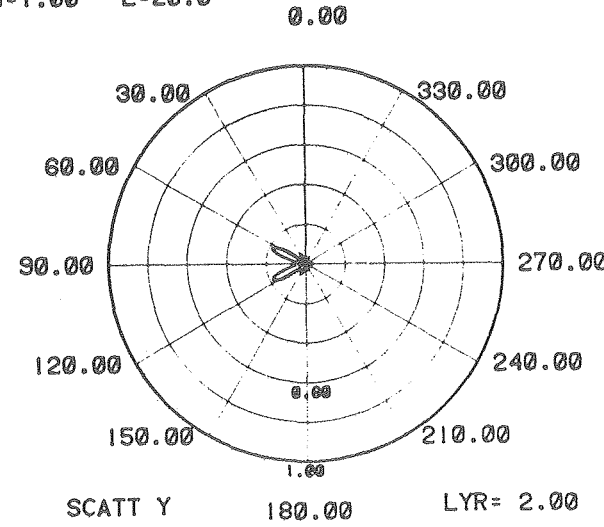
P=3.60 R=1.10
W=1.00 L=20.0



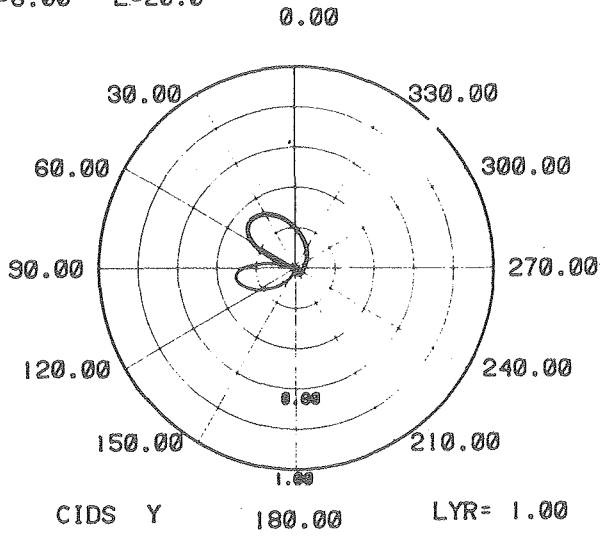
P=3.60 R=1.10
W=1.00 L=20.0



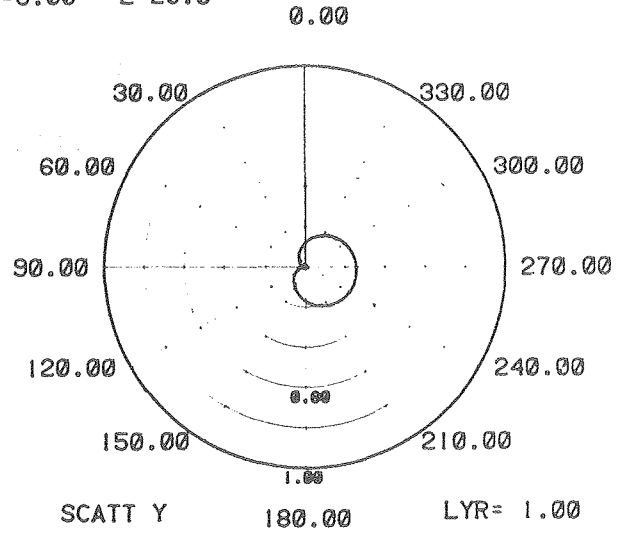
P=3.60 R=1.10
W=1.00 L=20.0



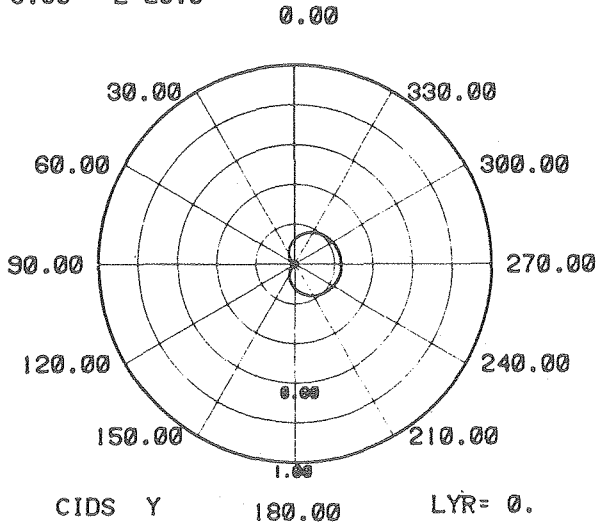
P=12.0 R= .60
W=6.00 L=20.0



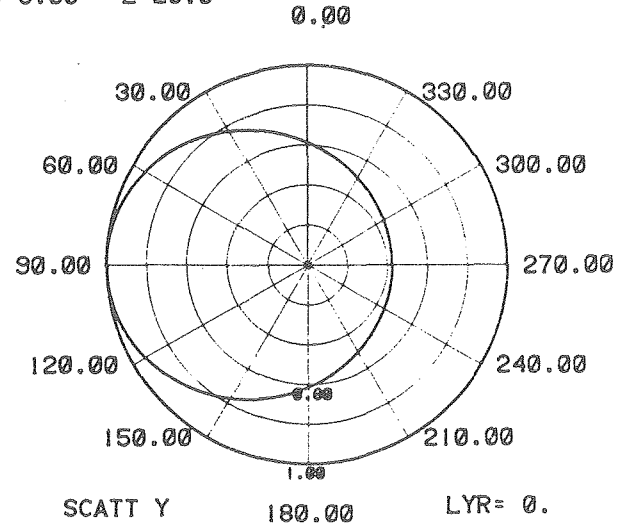
P=12.0 R= .60
W=6.00 L=20.0



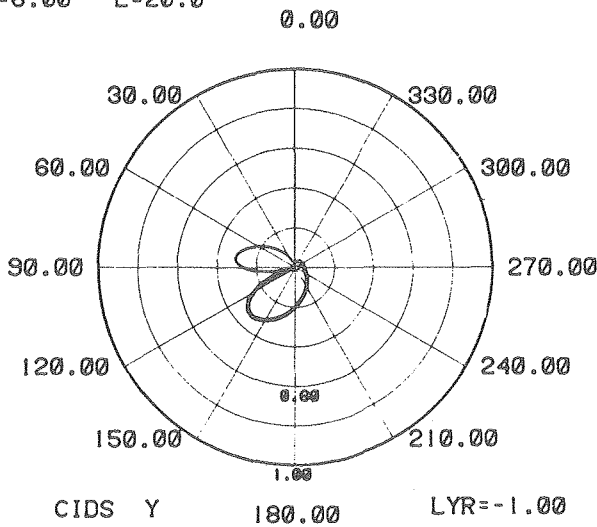
P=12.0 R= .60
W=6.00 L=20.0



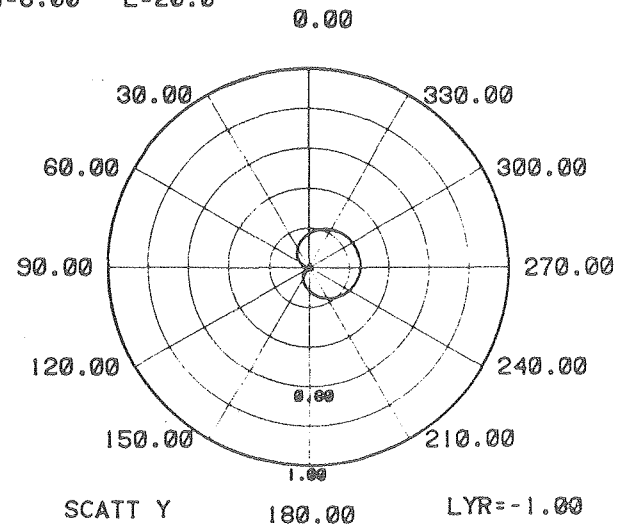
P=12.0 R= .60
W=6.00 L=20.0



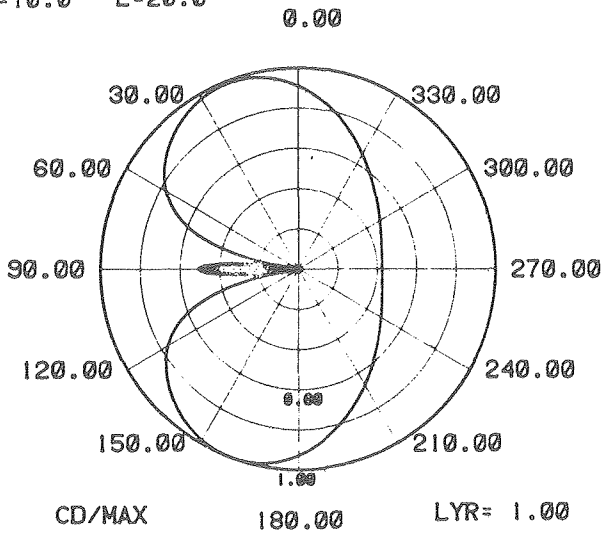
P=12.0 R= .60
W=6.00 L=20.0



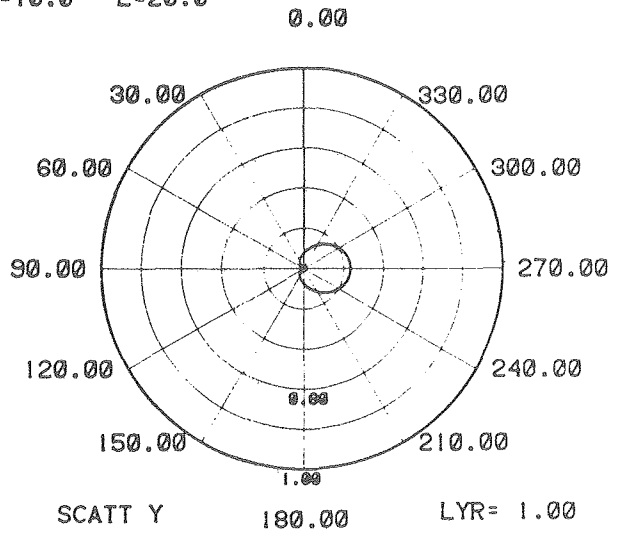
P=12.0 R= .60
W=6.00 L=20.0



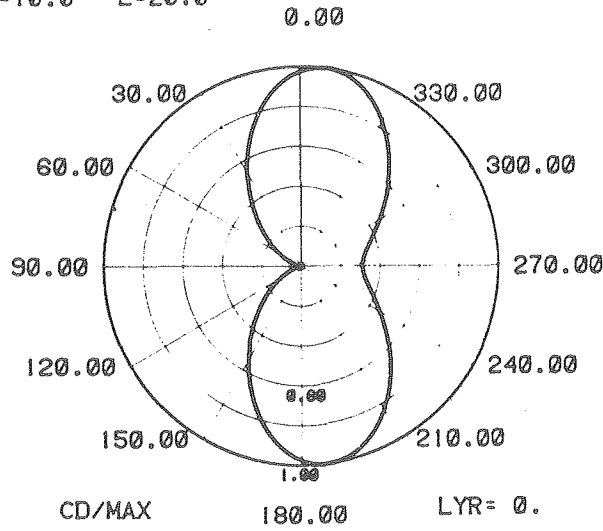
P=20.0 R=1.00
W=10.0 L=20.0



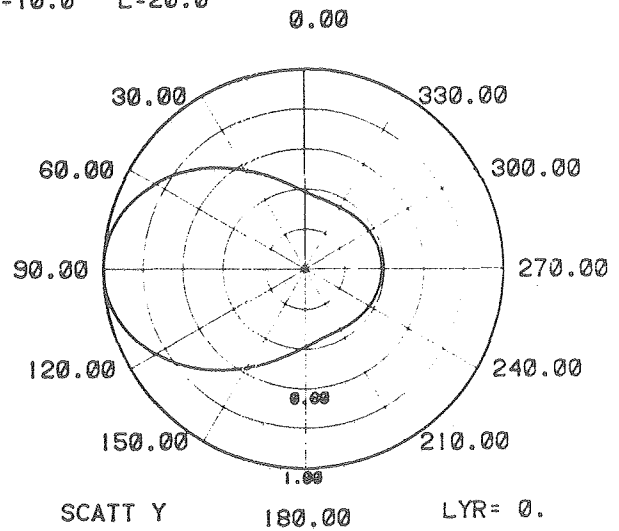
P=20.0 R=1.00
W=10.0 L=20.0



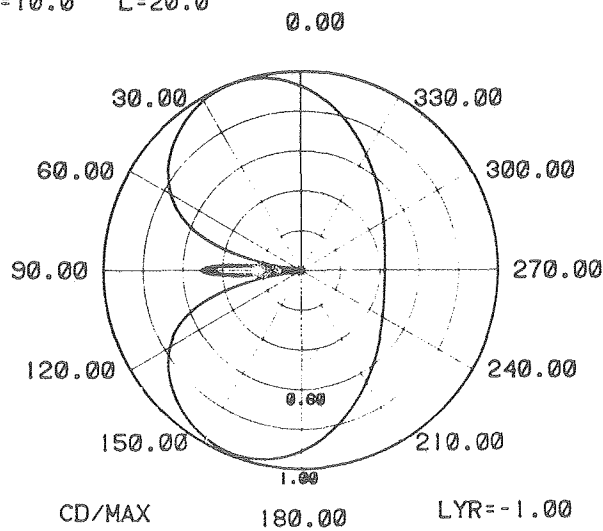
P=20.0 R=1.00
W=10.0 L=20.0



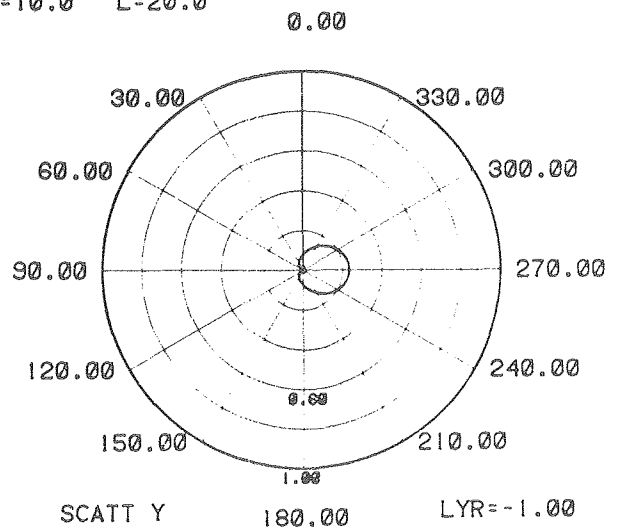
P=20.0 R=1.00
W=10.0 L=20.0



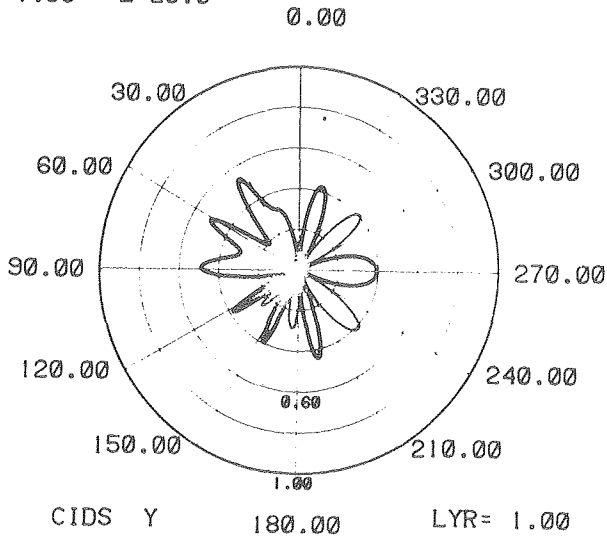
P=20.0 R=1.00
W=10.0 L=20.0



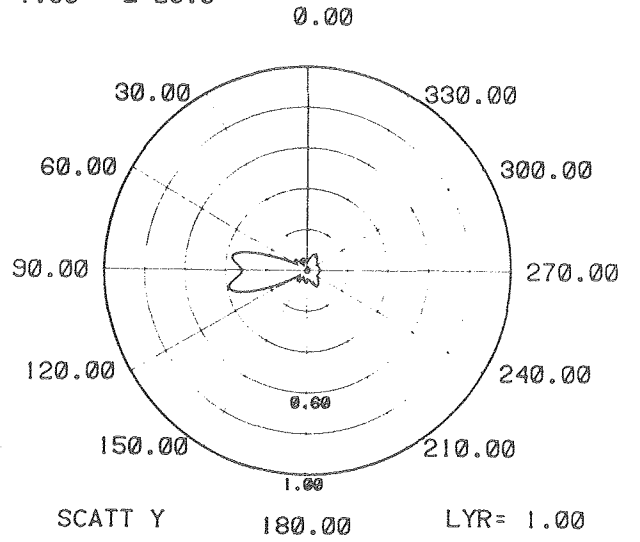
P=20.0 R=1.00
W=10.0 L=20.0



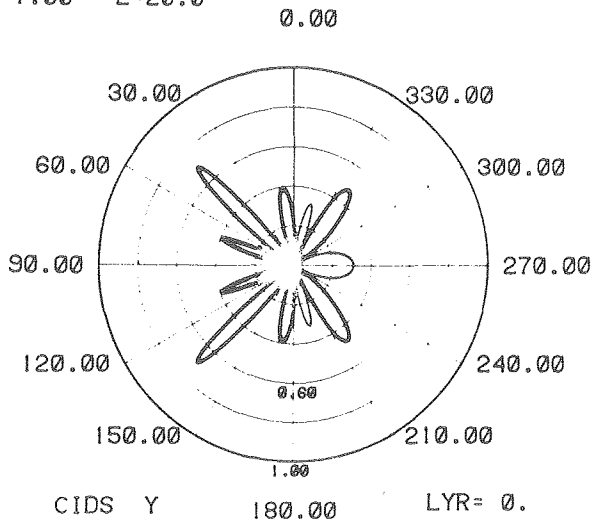
P=-3.6 R=1.10
W=1.00 L=20.0



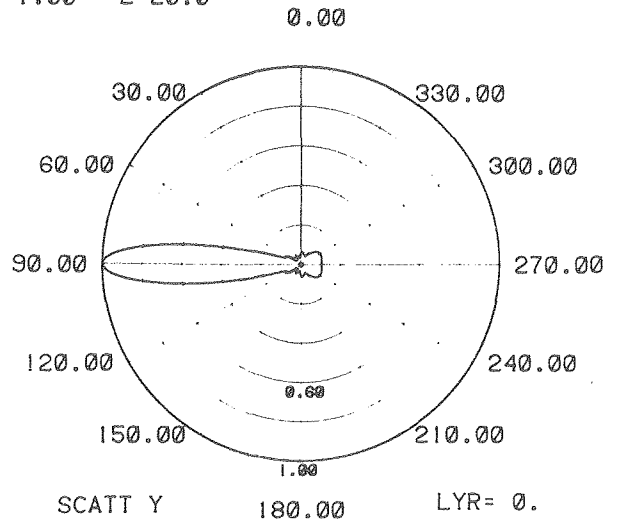
P=-3.6 R=1.10
W=1.00 L=20.0



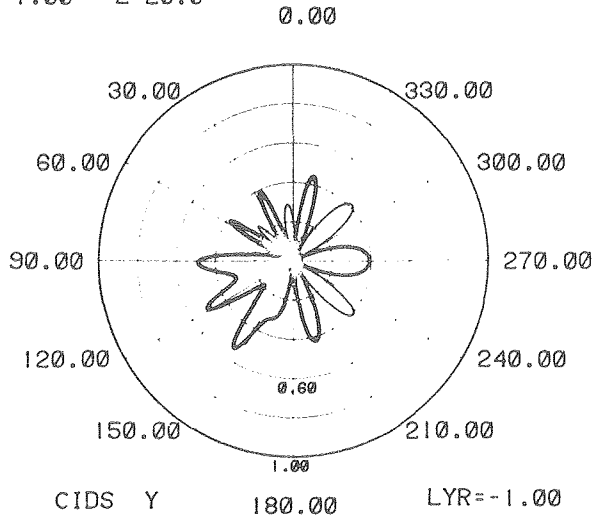
P=-3.6 R=1.10
W=1.00 L=20.0



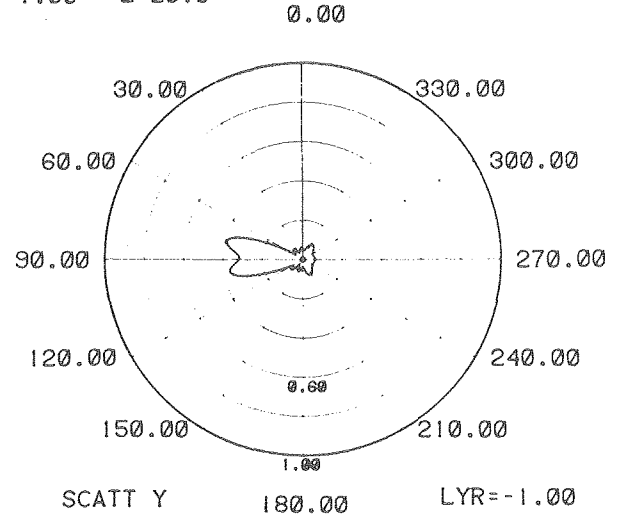
P=-3.6 R=1.10
W=1.00 L=20.0



P=-3.6 R=1.10
W=1.00 L=20.0

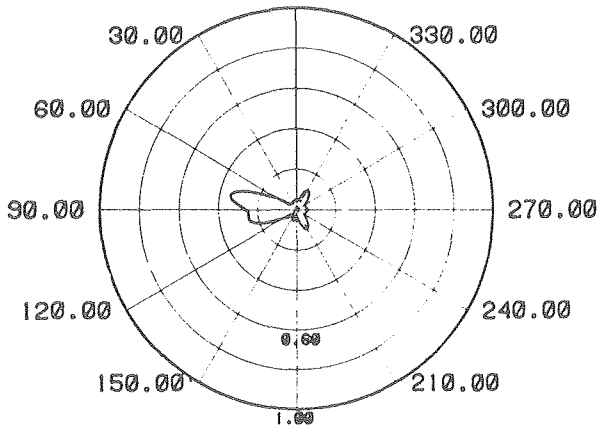


P=-3.6 R=1.10
W=1.00 L=20.0



P=3.60 R=1.10
W=1.00 L=20.0

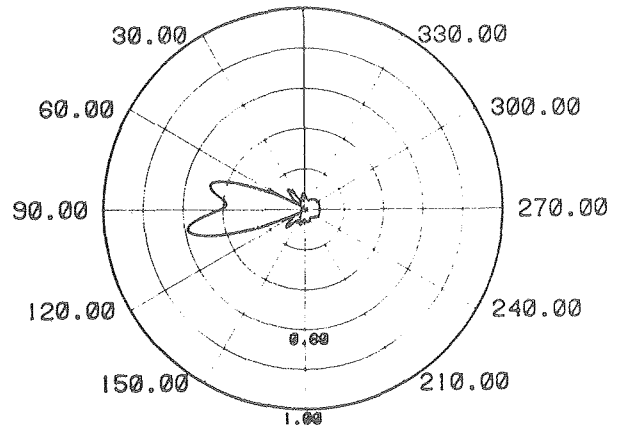
0.00



I POLX 180.00 LYR= 1.00

P=3.60 R=1.10
W=1.00 L=20.0

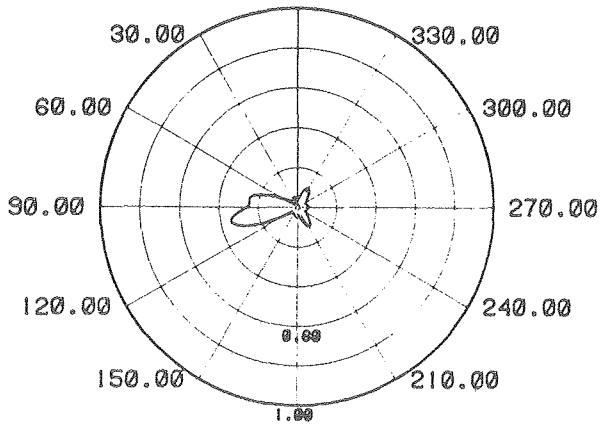
0.00



I POLZ 180.00 LYR= 1.00

P=-3.6 R=1.10
W=1.00 L=20.0

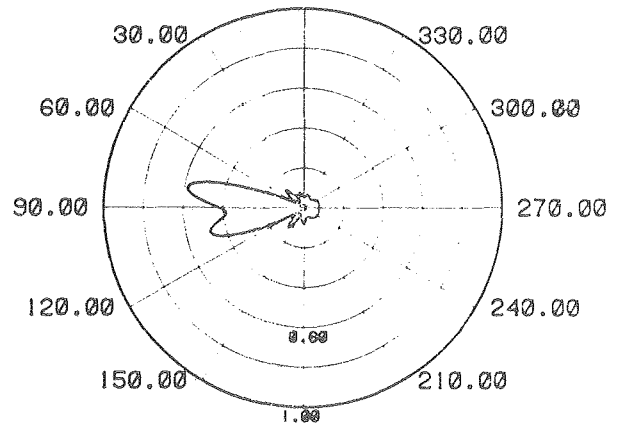
0.00



I POLX 180.00 LYR= 1.00

P=-3.6 R=1.10
W=1.00 L=20.0

0.00



I POLZ 180.00 LYR= 1.00